QUANTIFYING UNDERESTIMATES OF LONG-TERM UPPER-OCEAN WARMING

Paul J. Durack[1], Peter J. Gleckler[1], Felix W. Landerer[2] and Karl E. Taylor[1]

[1]Program for Climate Model Diagnosis and Intercomparison, Lawrence Livermore National Laboratory, Livermore, California, USA

[2]Jet Propulsion Laboratory, California Institute of Technology, Pasadena, California, USA

Draft: Monday, 14 July 14
Abstract = 173 words
Main text = 2417 words
Methods text = 627 words
Figure legends text (words): Fig1 = 97; Fig2 = 63; Fig3 = 108; Fig4 = 116; Fig5 = 139
References = 30

Corresponding author address: Paul J. Durack, Program for Climate Model Diagnosis and Intercomparison, Lawrence Livermore National Laboratory, Mail Code L-103, Livermore, California, USA 94550.
E-mail: pauldurack@llnl.gov

The global ocean stores more than 90% of the heat associated with observed greenhouse-gas-attributed global warming[1-4]. Using satellite altimetry observations and a large suite of climate models, we conclude that observed estimates of 0-700 dbar global ocean warming since 1970 are likely biased low. This underestimation is attributed to poor sampling of the Southern Hemisphere, and limitations of the analysis methods that conservatively estimate temperature changes in data-sparse regions[5-7]. We find that the partitioning of Northern and Southern Hemispheric simulated sea surface height changes are consistent with highly accurate altimeter observations, whereas the hemispheric partitioning of simulated upper-ocean warming is inconsistent with temperature observations. Relying on the close correspondence between hemispheric scale ocean heat content and steric changes, we adjust the poorly constrained observed Southern Hemisphere warming estimates to yield a hemispheric ratio consistent with the broad range of modelled results. These adjustments yield large increases (2.2-7.1 x 10^{22} J 35yrs^{-1}) to existing estimates of global upper-ocean heat change, and have important implications for sea-level, the planetary energy budget and climate sensitivity assessments.

Main

Numerous studies have examined the long-term (~1950-present) global mean and basin-scale evolution of ocean heat content (OHC) change in the upper 0-700 dbar[1,4,8-12] (See Supplementary Information) and important advancements have been made to correct for systematic measurement biases[6,13,14]. Evidence exists for a southward shift of the subtropical gyres and marked warming in the Southern Ocean[7,15-17], but limitations of methods used to "infill" these data-sparse regions may introduce a conservative bias toward low magnitude (zero) changes[5-7]. Several more recent estimates of OHC change attempt to address sampling deficiencies by relying on coincident sea surface height (SSH) estimates or the modern Argo array[8,9,12,18]. Additional ocean warming studies apply formal detection and attribution approaches that rely heavily on modelled estimates of intrinsic variability, and circumvent the use of infilled data by "subsampling" models in space and time, consistent with the sparse historical observations[19-22].

Here, we investigate the large-scale spatial structure of heat content changes in five observational estimates (derived independently with differing processing choices) that were evaluated in the IPCC Fifth Assessment Report[4]. Based on a series of consistency checks with high quality altimetry data and a large ensemble of climate models (Coupled Model Intercomparison Project phases 3 & 5), we find that observed Southern Hemisphere (SH) 0-700 dbar OHC changes are significantly underestimated, which in turn has important implications for sea-level and energy budget assessments. We analyse the 35-year period (1970-2004) over which both the CMIP5 "Historical" data

60 are available and during which observational sampling deficiencies are small enough to
61 yield reliable OHC changes, at least in the Northern Hemisphere (NH)[21].
62 OHC changes from the surface to 700 dbar are examined in four observational
63 estimates for which infilled gridded data was available[10,11,18,23] (Figure S2a; See
64 Methods). As an example, we show the Lev12[11] result (Figure 1: A1) alongside the
65 CMIP5 Historical multi-model mean (MMM, Figure 1: B1). To facilitate comparison of
66 the observed and simulated spatial structure of OHC changes, additional maps show
67 results with the global-average removed (Figure 1: A2, B2; Figure S2a: A2-E2). The
68 regions of inconsistency among the different datasets are highlighted by stippling, which
69 indicates where at least one of the four observational estimates disagrees in the sign of
70 the mapped change (Figure 1: A1, B1; Figure S2a: A1-D1, A2-D2), or where fewer than
71 75% of models agree with the MMM sign (Figure 1: B1, B2; Figure S2a: E1, E2; Figure
72 S2b: A2-D2, E2-I2). A prominent SH warming feature (30°S-50°S) is evident in MMM
73 trend maps (Figure 1: B1, B2; Figure S2b), in agreement with previous modelling
74 studies[24,25]. This strong warming, which is likely due to SH data sparsity and internal
75 variability that can mask the externally forced warming in this region, is much less
76 distinct in all observational analyses. In contrast to the single observational record, the
77 MMM averages across uncorrelated variability (Figure S2a: A2-D2).
78 Oceanographic theory[26] and models[24,25] (Figure 1: B2, Figure S2b) suggest that
79 shallow (above 700 dbar) ocean ventilation sites in the Southern Ocean (30-60°S) and
80 the North Atlantic will warm at a faster rate than the global mean ocean. These patterns
81 are broadly compatible with proxies of ocean ventilation, diagnosed from

82 concentrations of anthropogenic CFC-11 tracers in the observed ocean and are well
83 replicated by a limited CMIP5 model subset (Figure S3; see Supplementary Information).
84 Observational estimates of OHC are not completely independent as they share
85 data sources and in some cases apply similar processing procedures. The Ish09[10] and
86 Lev12[11] (Figure S2a: B1/2 & C1/2) datasets rely on similar objective analysis methods
87 and data sources (including XBTs, which require challenging bias corrections), and both
88 show a weak SH warming (compared to the NH), but a strongly warming North Atlantic.
89 These features are also present, though smaller in magnitude, in the Smi07[23] result
90 (Figure S2a: A1/2), which uses the covariance field obtained from the HadCM3 model to
91 infill gaps across sparsely sampled regions (see Supplementary Information). The
92 DW10[18] analysis, which is based on a smaller dataset of more accurate hydrographic
93 measurements (not including XBTs; Figure S2a: D1/2), suggests a more even warming,
94 with larger magnitudes in the South Pacific and South Atlantic basins compared to the
95 other observed analyses. In each of the four observed analyses, the Atlantic basin is
96 warming at a faster rate than the Pacific, with the largest values found in the well-
97 sampled North Atlantic, a feature also apparent in the CMIP ensembles (Figure 1: B1/2;
98 Figure S2b).
99 Although internal variability can explain a large portion of the discrepancy
100 between the observed and modelled estimates of OHC change (see Supplementary
101 Information), a contribution from systematic model or observational errors is also
102 possible. To investigate the influence of both model and observational biases, and to
103 test the physical consistency of model simulations, we compare simulated changes in

104 sea surface height (SSH) to highly accurate satellite altimetry measurements (see
105 Supplementary Information). SSH reflects ocean changes driven by steric expansion as
106 the oceans warm (accounting for approximately 40% of the long-term mean SSH
107 change[27]), along with mass contributions from the cryosphere, halosteric effects driven
108 by regional salinity changes and dynamic adjustments related to circulation changes. In
109 models where glacial melt waters are not represented, SSH changes on hemispheric
110 scales are almost entirely determined by full-depth steric changes, which are dominated
111 by the thermal component and therefore closely related to OHC changes (Figure 2,
112 Figure S4). Although the correspondence between simulated global mean SSH and OHC
113 is larger when the full ocean depth is considered (Figure 2), this strong correlation
114 persists for the more variable upper-ocean (0-700 dbar). The close correspondence
115 between OHC and SSH changes also holds at hemispheric scales (Figure 2), indicating
116 that the better observed steric anomalies can be used as a proxy for the hemispheric
117 partitioning of OHC change. A number of studies have relied on this relationship, and
118 have used observed SSH to inform infilling of the sparse temperature observations to
119 estimate global OHC changes[8,28] or inform estimates of sampling uncertainty[9,12] (see
120 Supplementary Information). The key benefit of SSH data is that contrary to poorly
121 sampled in-situ temperature, satellite altimetry provides near global coverage since late
122 1992 and measures observed SSH anomalies (relative to the reference period) with
123 sufficient precision to accurately monitor changes.
124 In the analysis that follows, we contrast changes between the NH and SH by
125 examining ratios of SH versus global changes for both OHC and SSH (see Methods). This

126 approach allows us to effectively calibrate in-situ temperature results between the
127 relatively well sampled NH and poorly sampled SH.

128 We compare hemispheric ratios of SSH to their OHC counterparts considering
129 linear trends over successively longer time scales. For the models and in-situ based OHC
130 estimates we begin all trend calculations in 1970, whereas for the observed SSH data we
131 begin in 1993 (Figure 3A, B). A fifth observational estimate of OHC Dom08[8,21] for which
132 hemispheric timeseries are available is also included. As expected, hemispheric trend
133 ratios are noisy on time scales of less than a decade due to significant interannual
134 variability, however by 1990 (20-year trends) they have largely stabilised and converged
135 (Figure 3A, B). Given the stability of these results, extending the model curves beyond
136 the end date of the simulations (2004) is unlikely to affect the results.

137 We also perform a similar analysis for the truncated time period (1993-present;
138 Figure 3C, D). Independent of the starting date, the observed SSH estimate lies well
139 within the range of inter-model ratios for the CMIP5 Historical simulations (MMM 0.62
140 vs inter-model standard deviation 0.50-0.73 Figure 3A; MMM 0.57 vs 0.45-0.69 Figure
141 3C). In contrast, the trends in the observed OHC ratio generally appear to be
142 substantially smaller than simulated by most models, although this discrepancy
143 decreases in recent years. The consistency between the observed and simulated SSH
144 ratios suggests that SH sampling errors in the observed OHC estimates have more of an
145 impact on the hemispheric partitioning than potential model biases.

146 All but one of the four observational OHC trend estimates in Figure 3B suggest a
147 much smaller SH contribution, with stabilised ratios at 15-years and longer time scales

148 well outside the inter-model standard deviation (MMM 0.56 and inter-model standard
149 deviation 0.50-0.63 vs 0.33-0.49 for observations Figure 3B). When considering a 1993
150 start date (Figure 3D), the OHC MMM trends stabilise within 10 years, whereas the
151 observational OHC ratios become progressively larger and toward better agreement
152 with the modelled estimates (MMM 0.53 and inter-model standard deviation 0.45-0.61
153 Figure 3D). This shift in the observed OHC trend is consistent with an increasing
154 influence of Argo data after 2004, at which point in-situ measurements begin to provide
155 near-global coverage[29]. With the dramatic increase in SH measurements there is less
156 need to infill, which in the earlier part of the record results in trends that are biased
157 low[5-7]. In other words, the observational trend ratios become more consistent with the
158 models as the SH data coverage improves, a result that is evident when comparing the
159 longer (1970-2012) versus the shorter (1993-2012) analysis period (Figure 3B vs D).
160 To summarise, the following tests build our confidence in the range of simulated
161 hemispheric ratios of OHC changes: (1) hemispheric SSH 20-year trend ratios are
162 consistent between CMIP simulations and high quality altimetry observations; (2) the
163 relationship between SSH and OHC is strong and robust for the spatial scales considered
164 (Figure 2); and (3) there is consistency between CMIP simulations and observed
165 estimates for the vertical partitioning of OHC change in the upper (0-700 dbar) and full
166 depth[30] (Figure 2, S4). We note that there is likely a small positive SH contribution to
167 observed SSH trends from a salinity (freshening) driven halosteric expansion[18], which
168 may account for some of the discrepancy between SSH and OHC ratios, however this
169 has little impact on our results.

A large number of model simulations from the CMIP3 20c3m and CMIP5 Historical experiments have been analysed to directly compare the SH versus globally integrated upper-ocean warming ratios to observations. According to models, SH OHC change contributes approximately half of the global total (the SH ocean covers 60% of the global ocean area) expressed by the MMM value of 0.59 (Figure 4). The discrepancy between models and observations is clear (0.59 versus 0.35-0.49; Figure 4), with the observational ratios largely inconsistent even when compared to each model experiment mean in isolation (black diamonds 0.52-0.58; Figure 4), or to a much larger composite distribution obtained from all available model simulations (633) across 9 CMIP experiments (Figure S8, light grey). The resolved model-based hemispheric ratio is insensitive to changes in forcing, as evidenced by comparing the 20c3m/Historical results to the strongly forced future experiments (e.g. SRESA2, RCP85) which include enhanced ocean stratification, mixed layer shoaling, and resulting changes to ocean ventilation rates (See Supplementary Information).

The SH contribution to the total upper OHC change found in the five observational datasets appears inconsistent with the large model ensembles (Figures 3B, 4), suggesting either a model or observational bias. However, the agreement between observed and simulated SSH changes, coupled with the close correspondence between OHC and SSH (Figure 2), and the better agreement of observed and simulated OHC for the recent Argo period (with improved SH coverage), suggests systematic model biases do not dominate results. We thus conclude that long-term observational

191 estimates of SH upper-ocean heat content change are biased low in agreement with
192 previous works[5-7].

193 We next evaluate the impact of the SH bias on global upper OHC change
194 estimates by assuming that the large distribution of model results accurately represents
195 the inter-hemispheric ratio of ocean heat uptake. We believe this approach is justified
196 by our comparisons of OHC and SSH (Figures 2, 3). By assuming the much better
197 sampled and more consistent observed NH OHC estimates (Figure S2a) are accurate, we
198 adjust the poorly constrained SH estimates (see Methods) so that they yield an inter-
199 hemispheric ratio that is consistent with the MMM (Figure 4). When this adjustment is
200 applied, the various observational estimates of 35-year global upper OHC change which
201 range from 5.0-12.9 x 10^{22} J are substantially increased in all cases. These adjusted
202 estimates span the range from 7.2-19.9 x 10^{22} J (Figure 5 inset; Observed ratios 0.35-
203 0.49 adjusted to 0.59; Figure 4). Depending on the observational analysis used, this
204 corresponds to 24-58% increases in the estimated global upper OHC change since 1970
205 and SH OHC increases of 48-166% (Figure 5; right bars). To provide perspective, for each
206 observational estimate we reapply our adjustment method using the modelled ratio
207 obtained from the distribution of simulations (Figure 4), and use a one standard
208 deviation spread to construct uncertainty bounds (Figure 5; inset, grey lines). We note
209 that the largest adjusted global values (Ish09[10], Lev12[11]) are consistent with a recent
210 upper OHC change estimate[12], and if uncertainty bounds are considered this agreement
211 includes four of the five adjusted values (Figure 5; upper inset).

212 We further investigate the consistency between observations and models by
213 considering the warming for each hemisphere separately (Figure 5, lower left and right
214 bars). We consider results from CMIP3 and CMIP5 separately (Figure 5 light and dark
215 grey bars), and show the one standard deviation spread (black lines) between available
216 CMIP5 Historical (dark grey bars) and CMIP3 20c3m (light grey bars) simulations. Using
217 this measure, only two of the five observations (Dom08[8], DW10[18]) appear consistent
218 with the modelled range for both hemispheres. All but one observed estimate (Smi07[23])
219 suggest a larger NH warming than the MMM values (Figure 5; left bars), and all five
220 observed estimates show a smaller SH warming than the MMM values (Figure 5; right
221 bars). The NH modelled changes are consistent with some, but not all observations, and
222 indicate that we cannot rule out an influence of model error on our adjustments.
223 Accurate estimates of global ocean warming are required to understand
224 contributions to observed sea-level and energy budget changes and to constrain
225 empirical estimates of climate sensitivity. Our analysis finds that modelled hemispheric
226 ratios of SSH changes are consistent with highly accurate altimetry observations but
227 remarkably inconsistent with in-situ based hemispheric ratios of OHC changes. Adjusting
228 the poorly constrained SH OHC estimates to yield an improved consistency with models
229 produces a previously unaccounted global upper OHC increase of 2.2-7.1 x 10^{22} J from
230 1970 to 2004 (Figure 5, upper inset). For perspective, these adjustments represent more
231 than double the 1970-2004 heat storage change for all non-ocean (terrestrial,
232 cryospheric and atmospheric) heat reservoirs combined[4], and highlights the importance
233 of accurately estimating ocean temperature change. By contrasting hemispheric

234 changes in an attempt to quantify the impact of SH observation deficiencies, our
235 analysis should motivate further work to construct improved estimates of global OHC
236 change.

Acknowledgements. The work of P.J.D., P.J.G. and K.E.T. from Lawrence Livermore National Laboratory is a contribution to the U.S. Department of Energy, Office of Science, Climate and Environmental Sciences Division, Regional and Global Climate Modeling Program under contract DE-AC52-07NA27344. The work of F.W.L. was performed at the Jet Propulsion Laboratory, California Institute of Technology under contract with NASA. We thank numerous colleagues from the Program for Climate Model Diagnosis and Intercomparison (PCMDI) for valuable feedback and input into this project. We also thank J. Durack of the University of California, San Francisco (USA), M. V. Durack of educAID (Australia), T.P. Boyer from the National Oceanographic Data Center, Silver Spring (USA), C.M. Domingues from the Antarctic Climate and Ecosystems CRC, Hobart (Australia), J.A Church from the Centre for Australian Weather and Climate Research, Hobart (Australia) and three anonymous reviewers for helpful comments on early drafts of this manuscript. We acknowledge the sources of observed data used in this study: D. Smith and J. Murphy (Smi07), C. Domingues (Dom08), M. Ishii and M. Kimoto (Ish09), S. Levitus and T. Boyer (Lev12) and the International Argo Program and the national programs that contribute to it. We acknowledge the World Climate Research Programme's Working Group on Coupled Modelling, which is responsible for CMIP, and we thank the climate modelling groups (listed in Tables S1 and S2) for producing and making available their model output. For CMIP the U.S. Department of Energy's Program for Climate Model Diagnosis and Intercomparison provides coordinating support and led development of software infrastructure in partnership with the Global Organization for Earth System Science Portals. The DW10 data presented in this study can be downloaded from the CSIRO Ocean Change website at www.cmar.csiro.au/oceanchange. LLNL Release #: LLNL-JRNL-651841.

Competing Interests. The authors declare that they have no competing financial interests

Authors' Contributions. P.J.D. completed the OHC analysis, P.J.G. assisted in the OHC analysis and F.W.L completed the SSH analysis. All authors assisted with interpretation and shared responsibility for writing the manuscript.

Author Information. Correspondence and requests for materials should be addressed to P.J.D. (pauldurack@llnl.gov)

Methods Summary

We constructed near-global annual mean interpolated maps of upper-ocean heat content (OHC) along with hemispheric timeseries for CMIP5 Historical (1970-2004), CMIP3 20c3m (1970-1999) and CMIP3/5 future model simulations (2065-2099), as well as for 5 available observations (1970-near present: Smi07[23], Dom08[8], Ish09[10], DW10[18] and Lev12[11]).

The hemispheric timeseries were computed with equal-area weighting from native model and observational grids and native land-sea masks which in most cases extend from 90°S - 90°N (Figure 3).

The mapped data is interpolated to a regular horizontal (70°S - 70°N) and vertical (0 – 700 dbar) grid for all models and observations, using an identical land-sea mask which excludes marginal seas, the Arctic Ocean and the high latitude Southern Ocean (Figure 1, S2a, S2b). After interpolation an iterative nearest neighbour infilling algorithm is employed to ensure the geographic coverage of each estimate is identical. We used a pre-computed hemispheric timeseries for the Dom08[8,21] analysis, as a gridded analysis was not available.

We contrast modelled and observational sea surface height (SSH) to assess the possible effect of model biases on our simulated hemispheric totals. SSH is analysed to investigate the internal consistency between ocean warming and total steric change, and we show these quantities are highly correlated over the hemispheric scales considered (Figure 2, S4). We consider the hemispheric contribution to global mean SSH changes in both models and observations and find these ratios show a strong

agreement. This strong hemispheric SSH agreement provides the motivation to assess modelled OHC and compare this to observed estimates.

We calculate the contribution to global upper OHC change obtained from the Southern Hemisphere (SH) alone, and contrast these ratios over the analysed period comparing the multi-model mean (MMM) for the CMIP3 20c3m and CMIP5 Historical simulations (R; Figure 4) and observations respectively. Guided by the observed and modelled consistency in SSH, we correct observations by scaling the SH/Global ratio to match the MMM ratio. This technique leverages the better-sampled observed Northern Hemisphere (NH) oceans and the SH/Global OHC ratio obtained from the model suite to provide a correction term (x) for the poorly constrained SH OHC estimate (SH_{Obs}). Once we have corrected the SH OHC estimate, we then use this (SH^{*}_{Obs}) along with the existing NH OHC estimate (NH_{Obs}) to recalculate the corrected global upper OHC total ($Global^{*}_{Obs}$) following (1-4) below:

$$R = \frac{SH_{Models}}{(SH_{Models} + NH_{Models})} = \frac{SH_{Obs} \times x}{((SH_{Obs} \times x) + NH_{Obs})} \quad (1)$$

$$x = \frac{R \times NH_{Obs}}{(1-R) \times SH_{Obs}} \quad (2)$$

$$SH^{*}_{Obs} = SH_{Obs} \times x \quad (3)$$

$$Global^{*}_{Obs} = SH^{*}_{Obs} + NH_{Obs} \quad (4)$$

To provide a measure of our correction uncertainty we use a one standard deviation spread of the SH/Global ratio from the available simulations (Figure 4). These are used to generate representative uncertainty error bars for our global OHC estimates

310 (Figure 5; upper inset, grey bars). We note that this provides a simplified uncertainty
311 estimate, however due to the large number of observational and model simulations
312 used in the study a more complex treatment of observational and modelled uncertainty
313 was not undertaken.

314 To enhance the model ensemble sample size, CMIP3 20c3m (1970-1999)
315 simulations and CMIP3 and CMIP5 future projections (2050-2099; SRES & RCPs) are also
316 sampled to assess the role of forcing on hemispheric ratios. Model drift was not
317 explicitly corrected, as drift is primarily an issue in the deeper ocean (>2000 dbar) and
318 correction considerably reduced the number of available simulations. Instead, we
319 calculated the impact of drift correction on a specific sub-suite of the CMIP5 Historical
320 simulations (Figure S10, S11). We found that for the drift-corrected model suite this
321 changed the MMM ratios by a negligible amount (<2%) and therefore the analysis was
322 found to be insensitive to drift correction. We note in the full-depth analysis which
323 compares OHC to total steric changes (Figure 2, panels D, E, F) is drift-corrected, which
324 accounts for spurious deep ocean anomalies and reduced available simulations from
325 162 (Figure S4) to 100.

326 For more detailed descriptions and supporting figures please refer to the
327 Supplementary Information.

References

1 Levitus, S., Antonov, J. & Boyer, T. Warming of the world ocean, 1955–2003. *Geophys Res Lett* **32**, L02604, doi:10.1029/2004GL021592 (2005).

2 Church, J. A. *et al.* Revisiting the Earth's sea-level and energy budgets from 1961 to 2008. *Geophys Res Lett* **38**, L18601, doi:10.1029/2011GL048794 (2011).

3 Otto, A. *et al.* Energy budget constraints on climate response. *Nature Geosci* **6**, 415-416, doi:10.1038/ngeo1836 (2013).

4 Rhein, M. *et al.* in *Climate Change 2013: The Physical Science Basis. Contribution of Working Group I to the Fifth Assessment Report of the Intergovernmental Panel on Climate Change* (eds T. F. Stocker *et al.*) Ch. 3, 255-315 (Cambridge University Press, 2013).

5 Gregory, J. M., Banks, H. T., Stott, P. A., Lowe, J. A. & Palmer, M. D. Simulated and observed decadal variability in ocean heat content. *Geophys Res Lett* **31**, L15312, doi:10.1029/2004GL020258 (2004).

6 Gouretski, V. & Koltermann, K. P. How much is the ocean really warming? *Geophys Res Lett* **34**, L01610, doi:10.1029/2006GL027834 (2007).

7 Gille, S. T. Decadal-Scale Temperature Trends in the Southern Hemisphere Ocean. *Journal of Climate* **21**, 4749-4765, doi:10.1175/2008JCLI2131.1 (2008).

8 Domingues, C. M. *et al.* Improved estimates of upper-ocean warming and multi-decadal sea-level rise. *Nature* **453**, 1090-1093, doi:10.1038/nature07080 (2008).

9 Lyman, J. M. & Johnson, G. C. Estimating Annual Global Upper-Ocean Heat Content Anomalies despite Irregular In Situ Ocean Sampling*. *Journal of Climate* **21**, 5629-5641, doi:10.1175/2008JCLI2259.1 (2008).

10 Ishii, M. & Kimoto, M. Reevaluation of historical ocean heat content variations with time-varying XBT and MBT depth bias corrections. *Journal of Oceanography* **65**, 287-299, doi:10.1007/s10872-009-0027-7 (2009).

11 Levitus, S. *et al.* World ocean heat content and thermosteric sea level change (0–2000m), 1955–2010. *Geophys Res Lett* **39**, L10603, doi:10.1029/2012GL051106 (2012).

12 Lyman, J. M. & Johnson, G. C. Estimating Global Ocean Heat Content Changes in the Upper 1800 m since 1950 and the Influence of Climatology Choice*. *Journal of Climate* **27**, 1945-1957, doi:10.1175/JCLI-D-12-00752.1 (2014).

13 Wijffels, S. E. *et al.* Changing Expendable Bathythermograph Fall Rates and Their Impact on Estimates of Thermosteric Sea Level Rise. *Journal of Climate* **21**, 5657-5672, doi:10.1175/2008JCLI2290.1 (2008).

14 Cowley, R., Wijffels, S., Cheng, L., Boyer, T. & Kizu, S. Biases in Expendable Bathythermograph Data: A New View Based on Historical Side-by-Side Comparisons. *Journal of Atmospheric and Oceanic Technology* **30**, 1195-1225, doi:10.1175/JTECH-D-12-00127.1 (2013).

15 Gille, S. T. Warming of the Southern Ocean Since the 1950s. *Science* **295**, 1275-1277, doi:10.1126/science.1065863 (2002).

16 Aoki, S., Bindoff, N. L. & Church, J. A. Interdecadal water mass changes in the Southern Ocean between 30°E and 160°E. *Geophys Res Lett* **32**, L07607, doi:10.1029/2004GL022220 (2005).

17 Alory, G., Wijffels, S. & Meyers, G. Observed temperature trends in the Indian Ocean over 1960–1999 and associated mechanisms. *Geophys Res Lett* **34**, L02606, doi:10.1029/2006GL028044 (2007).

18 Durack, P. J. & Wijffels, S. E. Fifty-Year Trends in Global Ocean Salinities and Their Relationship to Broad-Scale Warming. *Journal of Climate* **23**, 4342-4362, doi:10.1175/2010JCLI3377.1 (2010).
19 Barnett, T. P. *et al.* Penetration of Human-Induced Warming into the World's Oceans. *Science* **309**, 284-287, doi:10.1126/science.1112418 (2005).
20 AchutaRao, K. M. *et al.* Variability of ocean heat uptake: Reconciling observations and models. *Journal of Geophysical Research: Oceans* **111**, C05019, doi:10.1029/2005JC003136 (2006).
21 Gleckler, P. J. *et al.* Human-induced global ocean warming on multidecadal timescales. *Nature Clim. Change* **2**, 524-529, doi:10.1038/nclimate1553 (2012).
22 Pierce, D. W., Gleckler, P. J., Barnett, T. P., Santer, B. D. & Durack, P. J. The fingerprint of human-induced changes in the ocean's salinity and temperature fields. *Geophys Res Lett* **39**, L21704, doi:10.1029/2012GL053389 (2012).
23 Smith, D. M. & Murphy, J. M. An objective ocean temperature and salinity analysis using covariances from a global climate model. *Journal of Geophysical Research: Oceans* **112**, C02022, doi:10.1029/2005JC003172 (2007).
24 Banks, H. T. & Gregory, J. M. Mechanisms of ocean heat uptake in a coupled climate model and the implications for tracer based predictions of ocean heat uptake. *Geophys Res Lett* **33**, L07608, doi:10.1029/2005GL025352 (2006).
25 Fyfe, J. C. Southern Ocean warming due to human influence. *Geophys Res Lett* **33**, L19701, doi:10.1029/2006GL027247 (2006).
26 Talley, L. D. Shallow, Intermediate, and Deep Overturning Components of the Global Heat Budget. *Journal of Physical Oceanography* **33**, 530-560, doi:10.1175/1520-0485(2003)033<0530:SIADOC>2.0.CO;2 (2003).
27 Church, J. A. *et al.* in *Climate Change 2013: The Physical Science Basis. Contribution of Working Group I to the Fifth Assessment Report of the Intergovernmental Panel on Climate Change* (eds T. F. Stocker *et al.*) Ch. 13, 1137-1216 (Cambridge University Press, 2013).
28 Church, J. A., White, N. J., Coleman, R., Lambeck, K. & Mitrovica, J. X. Estimates of the Regional Distribution of Sea Level Rise over the 1950–2000 Period. *Journal of Climate* **17**, 2609-2625, doi:10.1175/1520-0442(2004)017<2609:EOTRDO>2.0.CO;2 (2004).
29 Roemmich, D. & Gilson, J. The 2004-2008 mean and annual cycle of temperature, salinity, and steric height in the global ocean from the Argo Program. *Prog Oceanogr* **82**, 81-100, doi:10.1016/j.pocean.2009.03.004 (2009).
30 Flato, G. *et al.* in *Climate Change 2013: The Physical Science Basis. Contribution of Working Group I to the Fifth Assessment Report of the Intergovernmental Panel on Climate Change* (eds T. F. Stocker *et al.*) Ch. 9, 741-866 (Cambridge University Press, 2013).

Figures

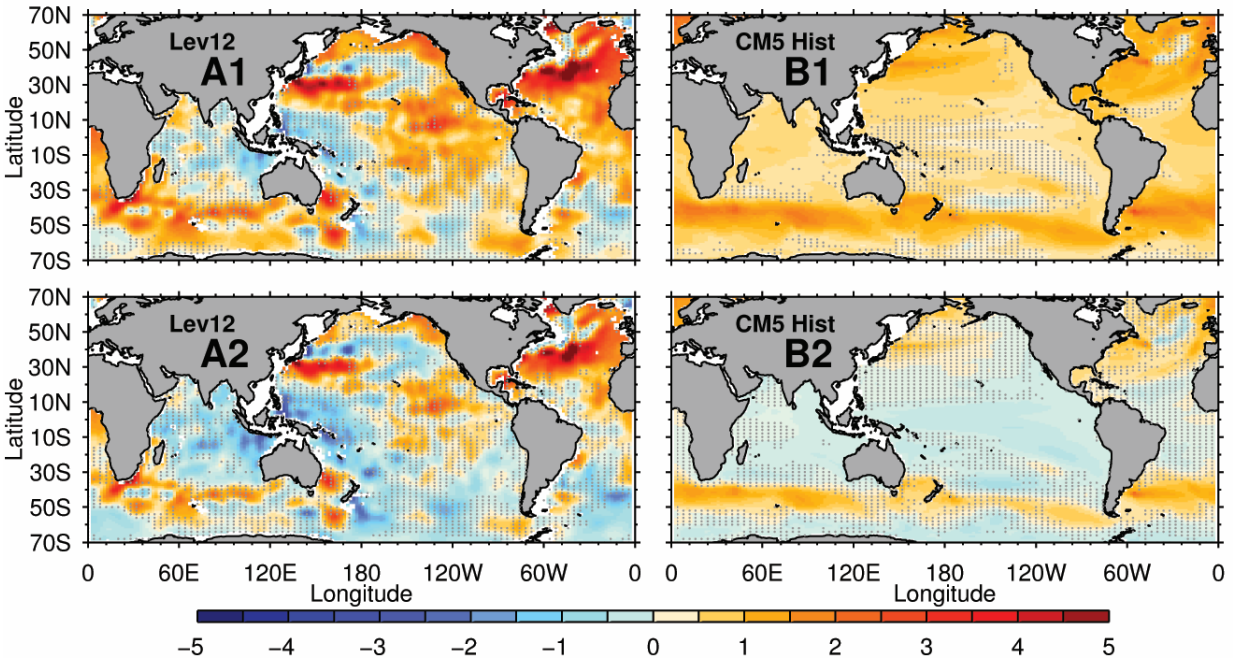

FIG. 1. 35-year (1970-2004) upper-ocean (0-700 dbar) heat content (OHC) trend maps (A1, B1; top row), and maps with the global mean removed (A2, B2; bottom row). Units are J x 10^3 kg^{-1} $35yrs^{-1}$ (4 ≈ 1°C $35yrs^{-1}$ depth-averaged warming). Observations are from Lev12[11] (A) and the CMIP5 Historical multi-model mean (MMM; B). Stippling marks regions where the 4 observational estimates do not agree in sign (A), and where <75% of models do not agree with the MMM sign (B). Maps for each observed estimate and for each CMIP experiment (MMM) are shown in Figure S2a and S2b respectively.

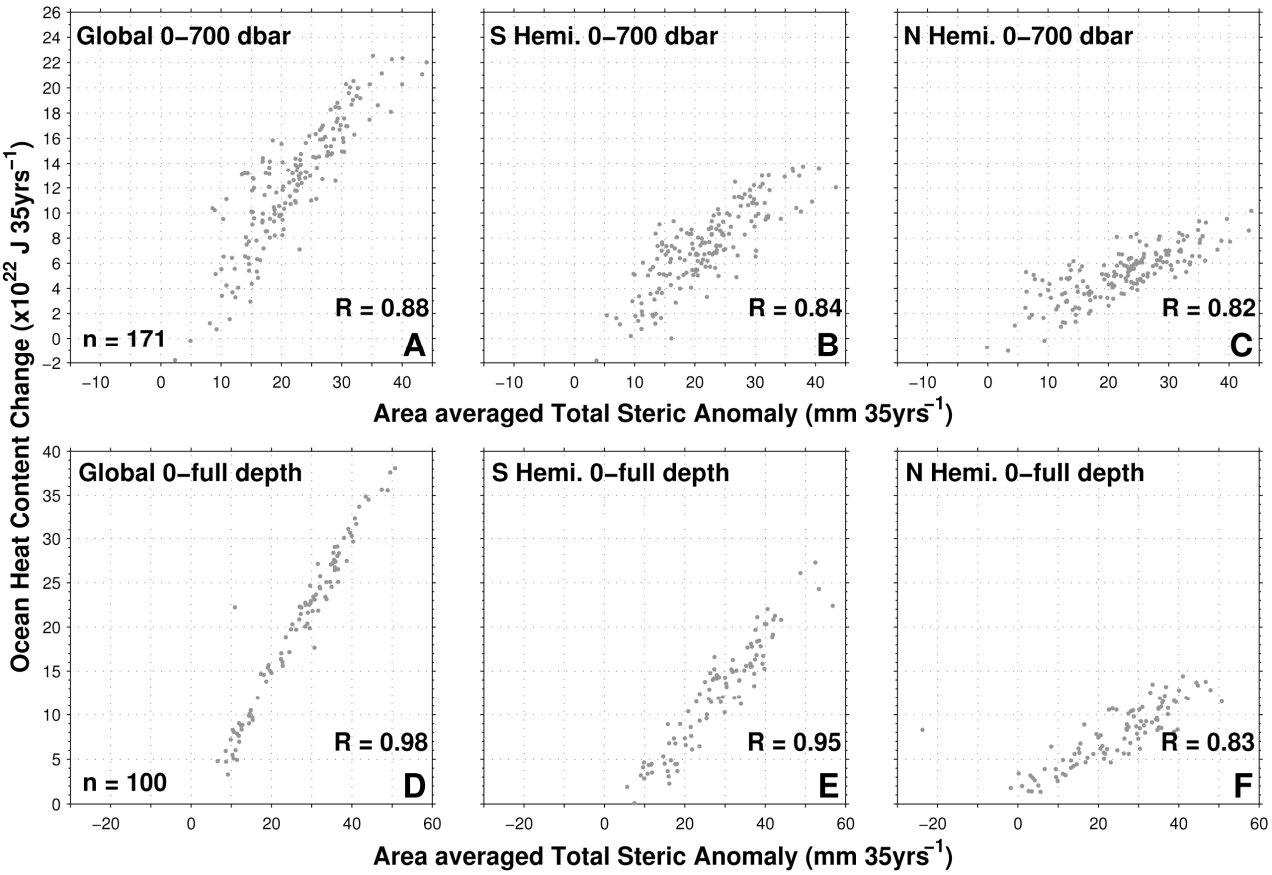

FIG. 2. Global and hemispheric depth-integrated 35-year trends in ocean heat content (OHC) change plotted against area-weighted average total steric anomalies (equivalent to sea surface height [SSH]) for CMIP5 Historical simulations in the upper 0-700 dbar (top row) and 0-full depth ocean (bottom row). Analysis that considers the full depth ocean (row 2) requires drift correction and consequently a smaller number of models were assessed.

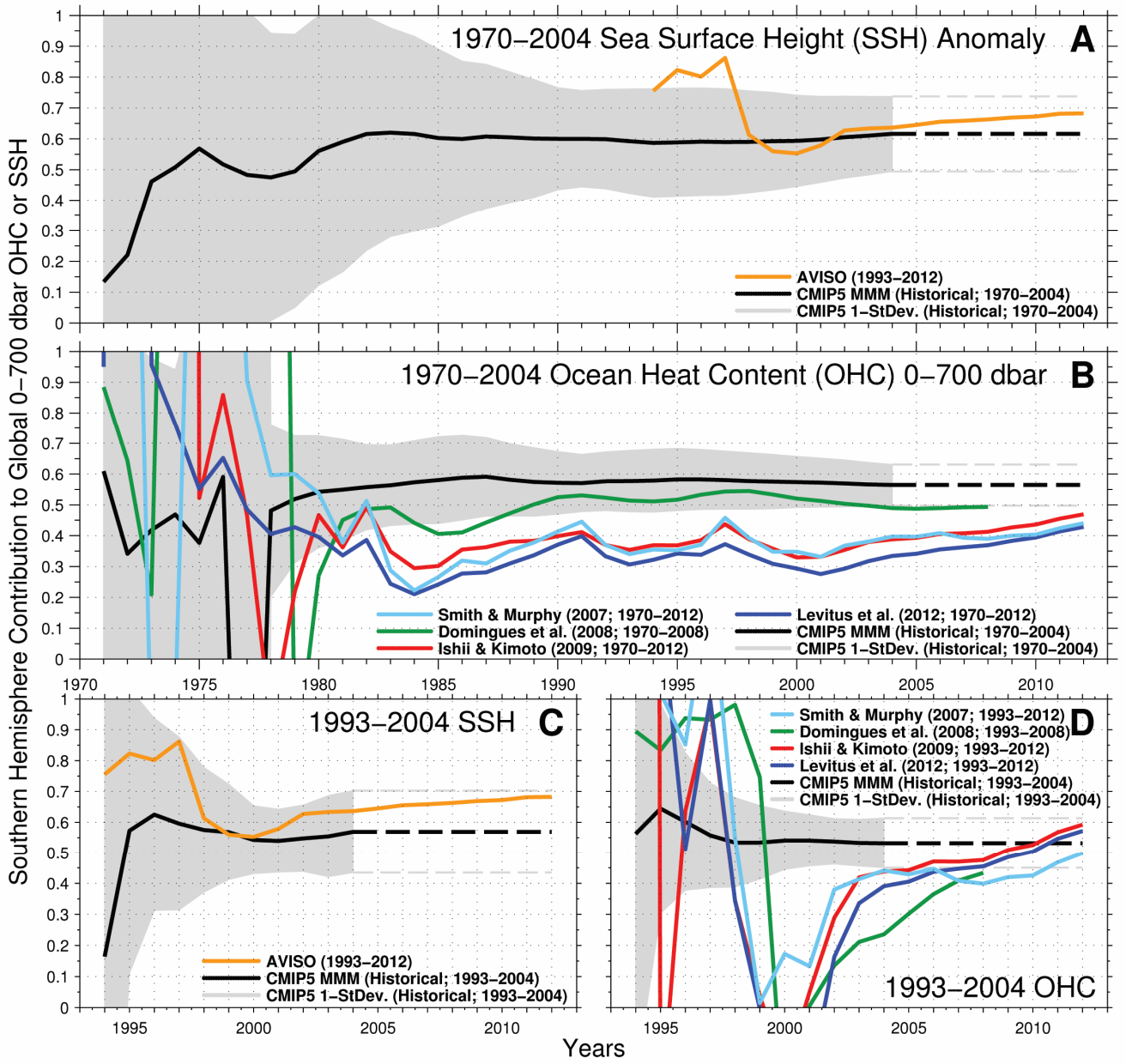

FIG. 3. Southern Hemisphere fractional contributions to global upper-ocean heat content (B, D) or globally averaged sea surface height anomaly (A, C) changes from varying trend lengths (1-35 years). Panels A and B show model results over 35-years (1970-2004). Panels C and D show model results for a shorter 11-year period (1993-2004) for which observed SSH data is available. Observed OHC results extend from 1970 to 2012 if available. Discontinuous black and grey lines extend 2004 CMIP5 values to 2012. The CMIP5 MMM and 1 standard deviation spread are obtained from Historical simulations. Results are obtained from hemispheric timeseries calculated from the native observation or model grid and land-sea mask.

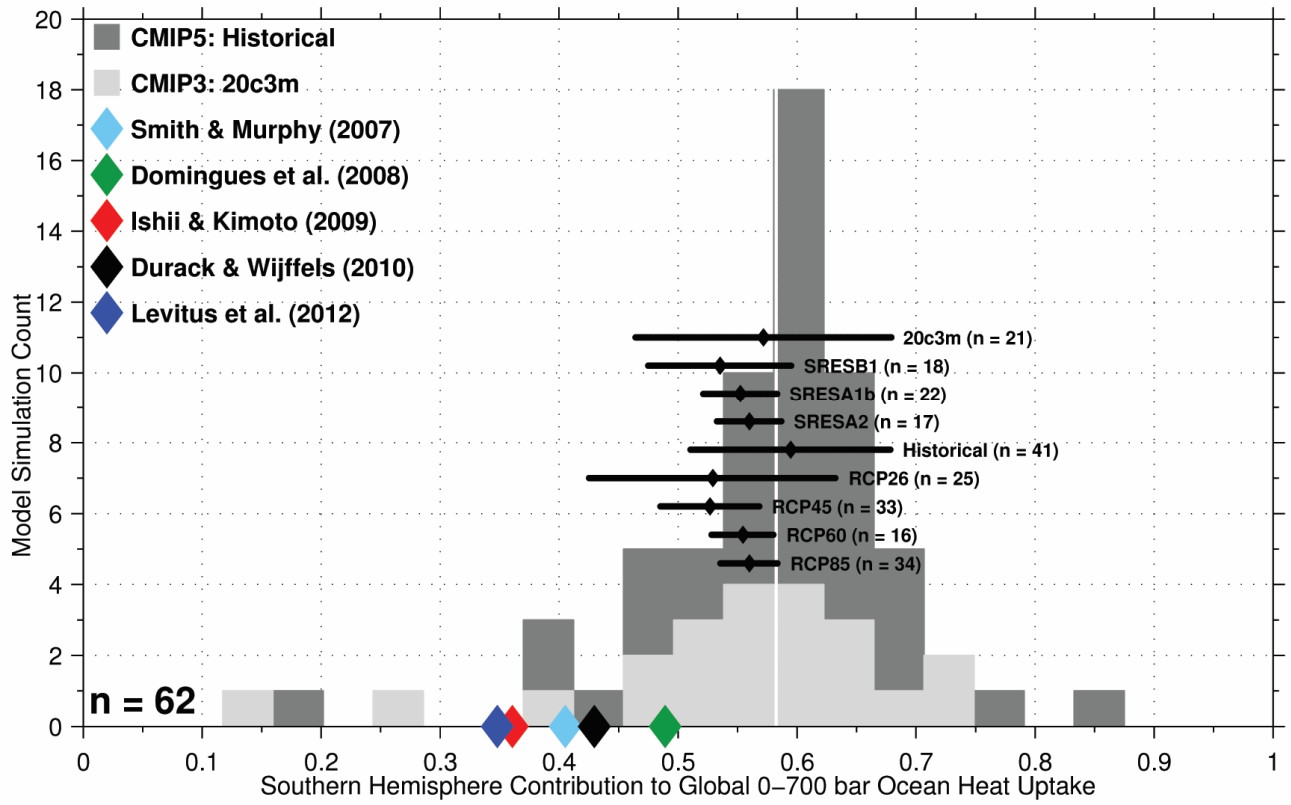

FIG. 4. Histogram of the Southern Hemisphere fractional contribution to the global upper-ocean heat content over 35-years (1970-2004) for observations and simulations. The distribution from 62 independent CMIP3 (20c3m) and CMIP5 (Historical) model means (average of single model simulations) is shown in dark grey (21 20c3m CMIP3; overlaid light grey). All CMIP experiment MMMs are shown (small black diamonds) with a 1 standard deviation spread (horizontal black line). The full ensemble MMM (dark grey) is presented as a vertical white line. Figure S8 shows composite single simulation distributions and S9 shows each CMIP experiment. Models are listed in Tables S1 and S2. Results are obtained from interpolated maps using an identical land-sea mask or from hemispheric timeseries (Dom08[8]).

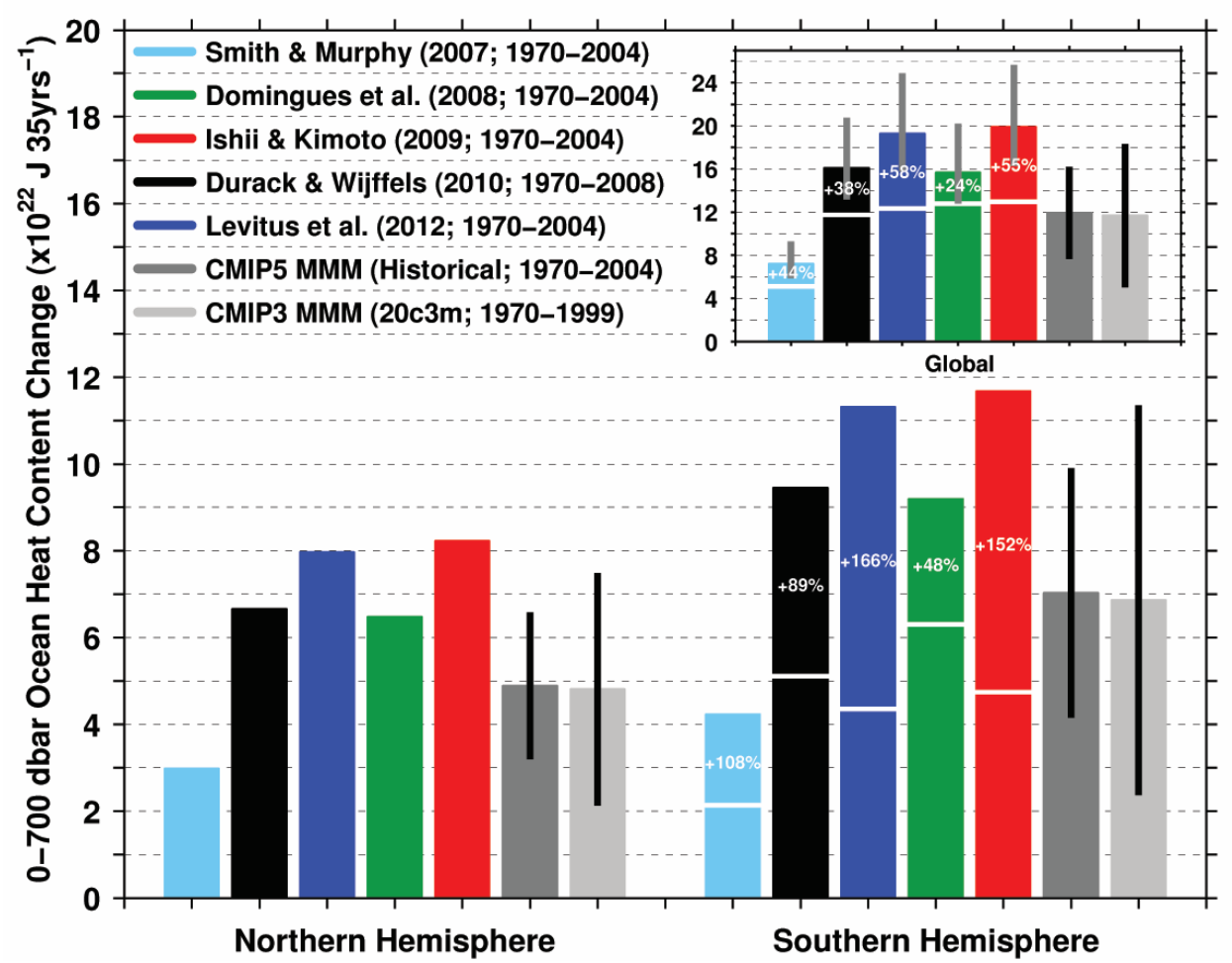

FIG. 5. Observed and simulated hemispheric and global 35-year (1970-2004) upper-ocean (0-700 dbar) heat content change. The one standard deviation spread in simulated estimates is given by the black lines. The SH unadjusted values (indicated by the white lines across the lower right bars) are adjusted to match the multi-model mean (MMM) hemispheric ratio of heat uptake found in CMIP3 20c3m and CMIP5 Historical simulations to obtain the full bar height. The NH and adjusted SH estimates are then summed to obtain global estimates (upper inset), and error bars (grey lines) show the range of adjusted values obtained considering the one standard deviation spread of model simulated ratios (Figure 4). The global unadjusted values are also indicated by the white lines across the inset bars. Even with the better coverage in the NH important observational differences are evident (lower left bars).